

A&A manuscript no.
(will be inserted by hand later)

Your thesaurus codes are:
02.01.1; 02.01.2; 02.16.2; 02.19.1; 11.03.1; 12.12.1

ASTRONOMY
AND
ASTROPHYSICS
26.1.2018

Cluster Radio Relics as a Tracer of Shock Waves of the Large-Scale Structure Formation

Torsten A. Enßlin¹, Peter L. Biermann¹, Ulrich Klein², Sven Kohle²

¹ Max-Planck-Institut für Radioastronomie, Auf dem Hügel 69, D-53121 Bonn, Germany

² Radioastronomisches Institut der Universität Bonn, Auf dem Hügel 71, D-53121 Bonn, Germany

Received ??? , Accepted ???

Abstract. We present evidence for the existence of shock waves caused by the formation of the large-scale structure. In some clusters of galaxies peripherally located sources of extended diffuse radio emission exist, the so-called cluster radio relics. They have steep radio spectra but no apparent cutoff, as old remnants of radio galaxies usually have. Therefore particle acceleration has to take place within them. We propose that shock structures of the cosmological large-scale matter flows are responsible for the acceleration of relativistic electrons: cluster accretion shocks and bow shocks of merger events. We develop a theory of radio plasma having traversed these shocks and compare it to observational data of nine radio relics (0038-096, 0917+75, 1140+203, 1253+275, 1712+64, 1706+78, 2006-56, 2010-57, 1401-33) and their host clusters (A85, A786, A1367, Coma, A2255, A2256, A3667, S753). The necessary accretion power, the spectral index of the radio spectrum, the acceleration efficiency of the shock, the diffusion coefficient in the post-shock region, and the predicted radio polarization in all of our examples fit into a coherent interpretation of the observational data. Since polarization measurements are available only for four sources, the predictions of our theory can be independently checked using other examples. The predicted values of the shock compression ratio, density and temperature of the infalling gas, magnetic field strength of the shocked and unshocked radio plasma are discussed within the frame of structure formation theory.

Key words: galaxies: clusters: general – shock waves – cosmology: large-scale structure of the Universe – accretion – acceleration of particles – polarization

1. Introduction

Large extended sources of synchrotron emission are found in some clusters of galaxies: radio halos and radio relics (Fig. 1; for reviews, see Jaffe 1992; Feretti & Giovannini 1996). The rare cluster *radio halo* phenomena are *large regions of diffuse unpolarized radio emission, centrally located*, and have radio structures roughly similar to that of the thermal X-ray emission (Deiss et al. 1997). The so-called *radio relics* are *peripherally located, and are more irregularly shaped polarized radio sources*. Radio relics are believed to be the remnants of radio lobes of radio galaxies, where the former active galaxy has become inactive or has moved away.

For radio halos a number of candidate sources for the relativistic, synchrotron emitting electrons were discussed in the literature (Schlickeiser et al. 1987 and references therein). Yet, the source of the energetic electrons in the relics is unclear, due to the shortness of the electron cooling time compared to the time since electron injection from a galaxy at the location of the relic was possible. Since the radio spectra of relics are steep but frequently do not exhibit any cutoff in the observed range, an efficient particle acceleration mechanism has to be present within or close to them. We show that shocks of the large-scale gas motion are expected at the typical peripheral locations of relics, either resulting from cluster mergers, or from steady state accretion shocks by gas falling into the cluster potential. Kang et al. (1997) showed that protons might be accelerated in cluster accretion shocks to energies comparable with the most energetic cosmic ray events observed at earth. Also electrons should be accelerated and become visible by radio emission at locations where magnetic fields are present. Therefore the magnetized plasma accumulated behind the shock or left behind as a remnant of a radio galaxy, could furnish this acceleration region and should also increase the efficiency of the acceleration mechanism. We demonstrate that for the case of the radio relic 1253+275 close to Coma A (Fig. 1), the observed spectral index and polarization of the radio

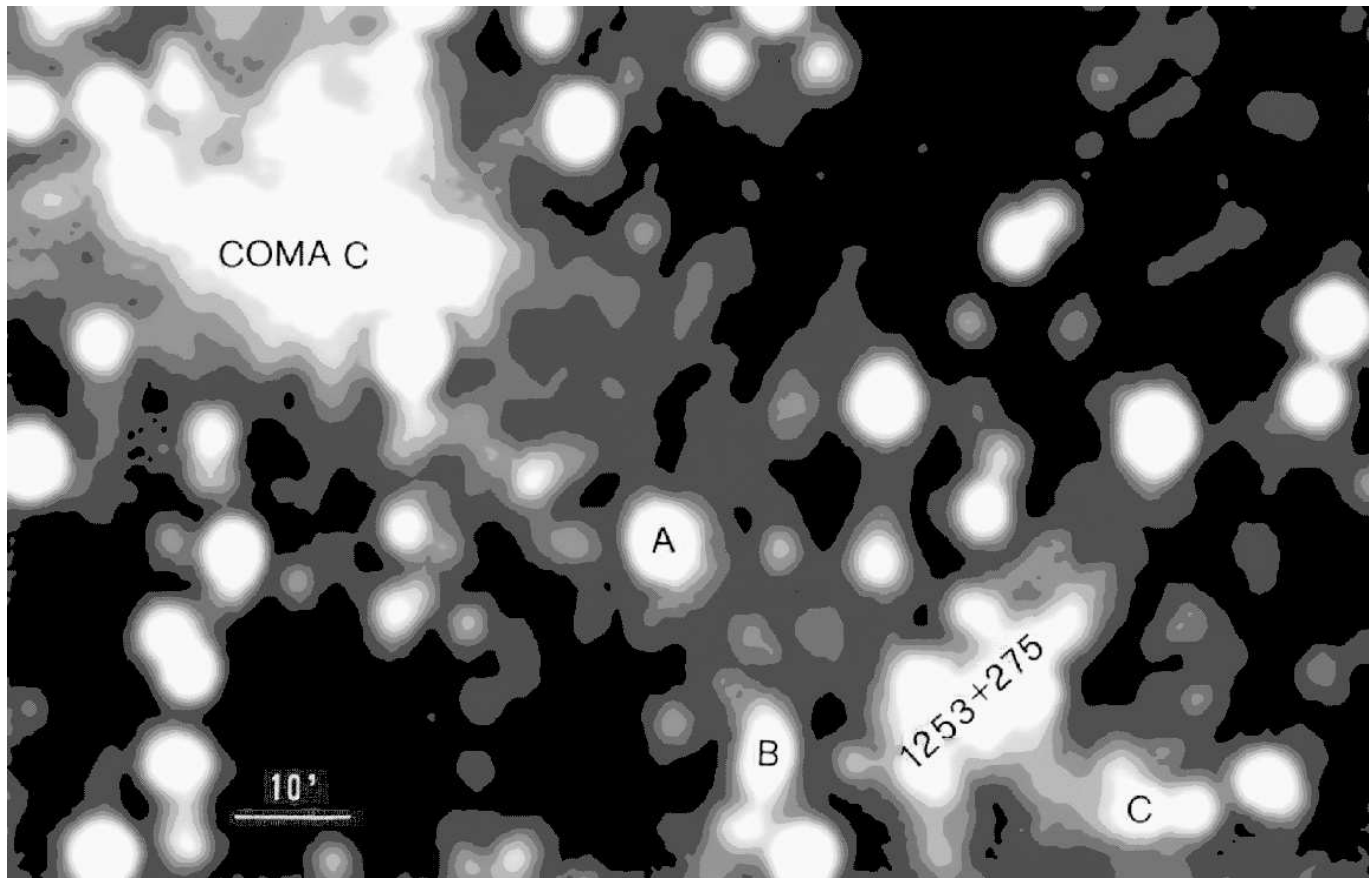


Fig. 1. Westerbork Synthesis Radio Telescope map at 327 MHz of the Coma cluster from Giovannini et al. (1991). The central halo source Coma C and the cluster relic 1253+275 are identified. Capital letters indicate some extended Coma cluster galaxies, as following: A = NGC 4839, B = NGC 4827, C = NGC 4789. 10' corresponds to 400 kpc h_{50}^{-1} .

emission agree well with the prediction for an accretion shock. Eight other relics are also briefly discussed.

We adopt for the following $\Omega_o = 1$ and $H_o = 50 h_{50} \text{ km s}^{-1} \text{ Mpc}^{-1}$.

2. Particle acceleration at cluster accretion shocks

2.1. Geometry

Properties of the accretion shocks of clusters of galaxies, the shock radius r_s and the velocity V_s of the infalling matter measured in the shock frame, are related to the depth of the gravitational potential of the cluster. Since the cluster gas temperature also depends on the potential, the shock properties can be expressed in terms of the observed temperature kT_{obs} . Using results of one-dimensional simulations of accreting flows onto clusters (Ryu & Kang 1997), Kang et al. (1997) derived

$$r_s = 4.24 h_{50}^{-1} \text{Mpc} \left(\frac{kT_{\text{obs}}}{6.06 \text{ keV}} \right)^{1/2} (1+z)^{-3/2} \quad (1)$$

$$V_s = 1750 \text{ km s}^{-1} \left(\frac{kT_{\text{obs}}}{6.06 \text{ keV}} \right)^{1/2} . \quad (2)$$

These estimates depend on the assumption of a spherical flow, of a polytropic index of the gas of $\gamma_{\text{gas}} = 5/3$, and they depend weakly on the assumed Einstein-de Sitter cosmology. Since the real infall pattern to clusters should be aspherical and correlated with the surrounding large-scale structure (Colberg et al. 1997), the shock radii and the shock velocities are expected to differ from these estimates. They might be regarded as average quantities, where from a single cluster can easily deviate. Inserting the X-ray temperature of the Coma cluster of 8.2 keV (Briel et al. 1992) and the redshift of $z = 0.0233$ (Fadda et al. 1996) gives a shock radius of $r_s = 4.8 h_{50}^{-1} \text{ Mpc}$ and a shock velocity of $2.0 \cdot 10^3 \text{ km s}^{-1}$. If 1253+275 is at the position of this shock, the projected distance to the cluster center of $2.9 h_{50}^{-1} \text{ Mpc}$ (Giovannini et al. 1991) implies an angle between line-of-sight and normal of the shock front of $\delta = 37^\circ$. The true angle is ambiguous ($180^\circ - \delta$ or δ), and depends on the location of the relic on the line-of-sight (foreground or background with respect to the cluster center). A possible configuration is sketched in Fig. 2, where the relic is located on the back side of the cluster accretion shock, since then a physical connection to the nearby radio galaxy NGC 4789 is possible as explained in Sect. 5.

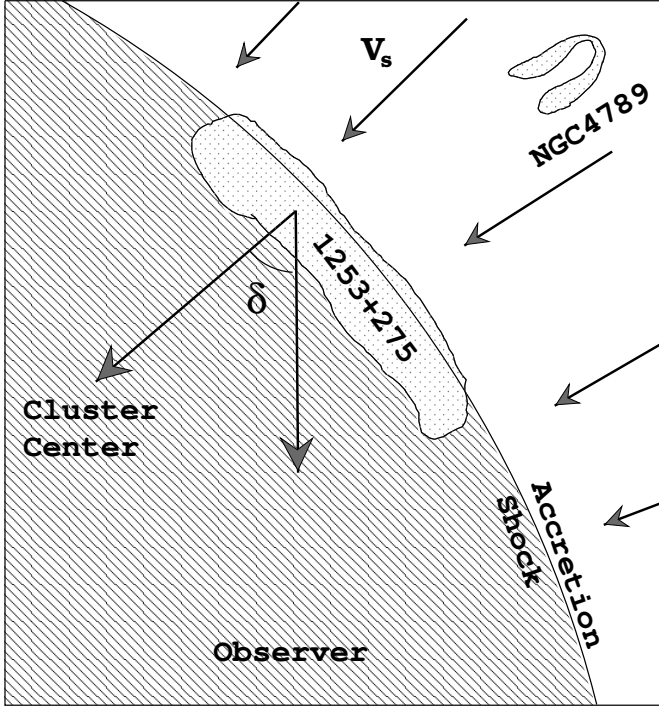


Fig. 2. Sketch of the assumed geometry in the Coma cluster. The accretion flow is indicated by arrows. The shaded region is the intra-cluster medium. The dotted area represents regions of radio plasma. The line-of-sight and the line connecting the relic and the cluster center are lying within the plane of the figure. NGC4789 is placed upstream above the radio relic as a source of relativistic electrons, as discussed in Sect. 5. Its line-of-sight velocity component points away from the observer. All positions could be different due to shifts parallel to the line-of-sight.

The length of the relic is $1.2 \text{ Mpc } h_{50}^{-1}$, whereas the thickness cannot be given directly from radio observations. We assume a thickness of $D = 0.1 \text{ Mpc } h_{50}^{-1}$, which is smaller than the observed projected thickness due to the action of shock compression in the infall direction. A detailed model of the structure of the relic would allow to deproject the apparent surface. For only moderately large projection angles ($\delta < 60^\circ$) resulting deprojected surfaces are not much bigger than the observed ones. Since the geometric quantities are only used for order of magnitude calculations of the infalling kinetic energy flux, the shock efficiency, and the diffusion coefficient within the radio plasma, we prefer not to specify a detailed geometrical model. We equate projected to real surface of the relic, which is a weak underestimate. The relic is slightly V-shaped and the radio emission is more sharply edged on the outer side (Giovannini et al. 1991). The V-shape could result from an aspherical shock, but would also be easily explained by an intrinsic shape of the magnetized plasma, since the relic is not seen edge-on. The edges of the observed projected radio structure should differ. The radio plasma seen at the

inner edge (left edge in Fig. 2) is more distant to the shock than that at the outer edge (right). The outer edge should be sharper due to the better confined plasma at the shock side, and it should have a lower than average spectral index, since the electrons there are reaccelerated recently. Whereas the inner edge is expected to be smoother and to have a higher than average spectral index. The reason for the latter is that the reaccelerated electrons within the radio plasma seen there, at a position more distant to the shock, had more time for cooling.

2.2. Compression ratio

The radio spectral index α ($S_\nu \sim \nu^{-\alpha}$) of 1253+275 is $\alpha = 1.18 \pm 0.06$ (Giovannini et al. 1991) and is therefore larger than $\alpha = 1$, expected for a strong shock accelerating electrons, with simultaneous synchrotron and inverse-Compton losses. Larger spectral indices are found at the inner edge of the relic, showing evidence for steepening of the electron momentum distribution due to the higher age of the electrons seen there, more distant to the acceleration region of the shock. The radius of the accretion shock structure (assumed to have a spherical surface) is large compared to every intrinsic length scale of the acceleration process. Thus the theory of planar shocks can be applied. The spectral index can be explained by allowing the shock compression ratio R to be lower than the canonical value $R = 4$ of a strong shock of gas with a polytropic index of $\gamma_{\text{gas}} = 5/3$. The radio spectral index α of an equilibrium electron population accelerated and cooled at the same time, is related to the shock compression ratio by (e.g. Drury 1983):

$$R = \frac{\alpha + 1}{\alpha - \frac{1}{2}}, \quad (3)$$

where a polytropic index of $\gamma_{\text{gas}} = 5/3$ is assumed. The compression ratio is therefore $R = 3.2 \pm 0.2$. From the theory of shocks (Landau & Lifschitz 1966) the pressure and temperature ratio between the down- and up-stream region (inside and outside the cluster shock front, in the following denoted by P_2 and P_1 , etc.) can be derived:

$$\frac{P_2}{P_1} = \frac{4R - 1}{4 - R} = \frac{\alpha + \frac{3}{2}}{\alpha - 1}, \quad \frac{T_2}{T_1} = \frac{1}{R} \frac{P_2}{P_1}. \quad (4)$$

For 1253+275 the resulting pressure ratio is $P_2/P_1 = 11 - 22$. The temperature ratio $T_2/T_1 = 3.8 - 6.4$ requires that the infalling matter has a temperature of $T_1 \sim 0.6 - 1.1 \text{ keV}$, assuming the post-shock temperature to be roughly half the central cluster temperature. Simulations predict this radial temperature decrease (Navarro et al. 1995), and observations indicate a radially falling temperature profile in clusters (Honda et al. 1996; Markevitch 1996; Markevitch et al. 1996, 1998).

This temperature of the infalling matter is reasonable, since this gas should flow mainly out of sheets and

filaments of the cosmological large-scale structure, and therefore was preheated by the accretion shocks at the boundaries of these structures. A simulation of cosmological structure formation by Kang et al. (1996) shows that typical temperatures of filaments are above 0.1 keV. Adiabatic compression and internal shocks within the flows onto clusters might raise these temperatures to a level of 0.5 – 1 keV, which is needed in order to explain the steepness of the synchrotron spectrum of cluster relic sources caused by weak shocks.

The temperature of the infalling matter gives the sound velocity c_1 , which enters into a second estimate of the shock velocity, using the theory of planar shock waves (Landau & Lifschitz 1966):

$$V_{s,\text{predicted}} = c_1 \sqrt{\frac{(\gamma_{\text{gas}} - 1) + (\gamma_{\text{gas}} + 1)P_2/P_1}{2\gamma_{\text{gas}}}}. \quad (5)$$

This estimate gives a shock velocity for Coma of $V_{s,\text{predicted}} = 1850$ km/s, slightly smaller than that following from the theory of Kang et al. (1997). The difference vanishes if a smaller temperature drop of ≈ 1.6 from the center to the shock radius is used instead of a factor of 2. Comparing both estimates shows self-consistency of our model, but this is not a completely independent test, since both values depend mainly on the same quantity ($V_s \sim (kT_{\text{obs}})^{1/2}$).

In the model of acceleration of ultra-high-energy cosmic rays at cluster accretion shocks of Kang et al. (1997) a compression ratio close to $R = 4$ is favored in one particular model to fit the shape of the spectrum of ultra-high-energy cosmic rays using a low and energy independent escape efficiency of cosmic rays from the cluster against the upstream flow. However, a lower compression ratio (and therefore a steeper cosmic ray production spectrum) can be compensated by taking a reasonable energy dependence of the escape efficiency into account. In fact, in Kang et al. (1997) the acceleration and escape efficiency was rather low, with $\approx 10^{-4}$ giving a reasonable fit only to the observed high-energy cosmic ray data. Using the compression ratio of $R = 3.2 \pm 0.2$ gives a proton spectrum of $E^{-2.36 \pm 0.12}$ implying for the same flux at a few 10^{19} eV a combined efficiency which is in the range 0.03 – 0.1 (Fig. 5 in Kang et al. 1997) and so consistent with estimates for supernova remnants (e.g. Drury et al. 1989; Völk 1997).

2.3. Shock Efficiency

A rough estimate of the gas densities on both sides of the shock sphere can be gained by extrapolating the electron density profile of the Coma cluster, viz. $n_e = n_{e,o} [1 + (r/r_{\text{core}})^2]^{-3\beta/2}$, with the parameters $n_{e,o} = 3 \cdot 10^{-3} h_{50}^{-1/2} \text{cm}^{-3}$, $r_{\text{core}} = 400 h_{50}^{-1} \text{kpc}$, and $\beta = 0.75$ (Briel et al. 1992). This gives a gas density of the order $n_{e,2} \approx 10^{-5} h_{50}^{-1/2} \text{cm}^{-3}$ at a cluster radius of $4.8 h_{50}^{-1} \text{Mpc}$. The density of the infalling matter should therefore be of

the order of $n_{e,1} \approx 3.5 \cdot 10^{-6} h_{50}^{-1/2} \text{cm}^{-3}$. This is consistent with the somewhat lower gas density in the intergalactic space of $\leq 10^{-6} \text{cm}^{-3}$ far away from clusters, derived e.g. from radio observation of the giant radio galaxy 1358+305 (Parma et al. 1996).

The projected extent of 1253+275 is $1.2 \times 0.4 h_{50}^{-2} \text{Mpc}^2$ (Giovannini et al. 1991), but its real surface S exposed to the accretion flow might be larger. The kinetic power of the infalling matter on the relic

$$Q_{\text{flow}} = \frac{1}{2} n_{e,1} m_p \tilde{V}_s^2 V_s S \approx 5 \cdot 10^{43} h_{50}^{-3/2} \text{erg s}^{-1}, \quad (6)$$

is mainly transformed into thermal energy, but some fraction is converted into relativistic particles. $\tilde{V}_s = V_s (R - 1)/R$ is the velocity of the infalling matter measured in the cluster's inertial frame. The integrated radio power between 10 MHz and 10 GHz of $8 \cdot 10^{40} h_{50}^{-2} \text{erg s}^{-1}$ (Giovannini et al. 1991) is three orders of magnitude lower, and can be easily powered by the dissipative processes in the shock. Assuming a field strength of $1 \mu\text{G}$ implies that only 10% of the electron radiation losses are synchrotron emission, the rest are inverse Compton losses by scattering of microwave background photons. The amount of energy loss of the electrons $Q_{\text{loss}} \approx 8 \cdot 10^{41} h_{50}^{-2} \text{erg s}^{-1}$ and the power of the flow Q_{flow} onto the relic gives the necessary minimal efficiency of shock acceleration. The efficiency needs to be higher than 1% in order to account for the radiative energy requirements and for escaping electrons. This number might be compared to the efficiency of shock acceleration in other astrophysical objects: It is believed that supernova blast waves have efficiencies of 1% – 10% for the acceleration of protons as is necessary in order to explain the galactic cosmic rays below 10^{15} eV by supernovae (e.g. Drury et al. 1989; Völk 1997). This shows that the assumed cluster efficiency is reasonable.

2.4. Electron Spectrum

We apply the theory of plane-parallel shock acceleration, because of the large radius of the shock sphere. We mark upstream quantities with index 1, and downstream quantities with index 2. We use a momentum independent diffusion coefficient, because of the success of this simplification in other circumstances (Biermann 1993, 1996; Wiebel-Sooth et al. 1997). The distribution function of the accelerated electrons cooling by inverse Compton and synchrotron emission is

$$f(x, p) = C p^{-q} \exp(-p/p^*(x)) \quad (7)$$

(Webb et al. 1984), where the normalization C can be approximated by being independent of the position x , and $q = 3R/(R - 1)$ is the spectral index of the injection electron distribution in three-dimensional momentum space. The cutoff momentum is

$$p^*(x) = \frac{4p_o}{q/a_1 + (q - 3)/a_2 + |x|U/(\kappa a)}$$

$$=: (F + |x|G)^{-1}, \quad (8)$$

with U denoting the flow velocity in the inertial frame of the shock ($U_1 = V_s$ and $U_2 = U_1/R$), κ is the diffusion coefficient, p_o is the injection momentum into the acceleration mechanism, and a is the ratio between loss and acceleration time scale:

$$a = \frac{U^2 m_e c \tau_{\text{loss}}}{4 \kappa p_o} \quad (9)$$

The energy loss time scale $\tau_{\text{loss}} m_e c/p$ of an electron with momentum p is dominated by synchrotron and inverse-Compton losses with:

$$\tau_{\text{loss}}^{-1} = \frac{4\sigma_T}{3m_e c} \left(\frac{B^2}{8\pi} + \varepsilon_{\text{ph}} \right), \quad (10)$$

where ε_{ph} is the energy density of the photon field, which is dominated by the microwave background. In Sect. 3.4 it is argued that the main fraction of the synchrotron emitting volume belongs to the post-shock region. Thus the electron population, integrated over the synchrotron emitting relic volume $\text{Vol} = SD$ (where S is the surface area, and D is the thickness), can be assumed to be

$$\begin{aligned} f(p) &= S \int_0^D dx f(x, p) \\ &= \frac{SC}{G_2} p^{-(q+1)} \exp(-pF) [1 - \exp(-pG_2D)]. \end{aligned} \quad (11)$$

This spectrum has a break at $p_{\text{break}} = 1/(G_2D)$ between the spectral index q and $q+1$, and a cutoff at $p_{\text{cut}} = 1/F$. The break in the momentum spectrum at

$$p_{\text{break}} = \frac{m_e c U_2 \tau_{\text{loss},2}}{D} \quad (12)$$

leads to a break in the radio spectrum at $\nu_{\text{break}} = 3eB_2 p_{\text{break}}^2 / (2\pi m_e^3 c^3)$. Using this relation and solving Eq. 12 for the ratio D/U_2 , which is the time the magnetized plasma needed to pass the shock, and therefore the age of the relic as a tracer of the shock structure, we get

$$t_{\text{age}} = \frac{D}{U_2} = \sqrt{\frac{3eB_{2,\text{eq}} m_e c}{2\pi \nu_{\text{break}}}} \left[\frac{4}{3} \sigma_T \left(\frac{B_{2,\text{eq}}^2}{8\pi} + \varepsilon_{\text{ph}} \right) \right]^{-1}. \quad (13)$$

We use a thickness of $D = 100 h_{50} \text{ kpc}$, roughly $\frac{1}{4}$ of the width of the projected structure of 1253+275, due to compression. The age of 1253+275 being a shock-tracer estimated from the kinematics $t_{\text{age,kin}} = DR/V_s = 1.5 \cdot 10^8 \text{ yr } h_{50}^{-1}$, and that following from Eq. 13: $t_{\text{age,break}} > 4 \cdot 10^8 \text{ yr}$, using the lowest observation frequency of 151 MHz as an upper limit to the break frequency ν_{break} , do not fit exactly. Regarding the approximations of this theory, and the uncertainties of the observational quantities only an order of magnitude accordance can be expected. But since these two estimates of the relic age depend on

different observational quantities ($t_{\text{age,kin}}(kT_{\text{obs}}, \alpha, D)$ and $t_{\text{age,break}}(\nu_{\text{break}}, B_{2,\text{eq}})$), this is a further test of the theory, which could have failed by orders of magnitude. Reasons for a discrepancy might also be hidden in neglected properties of the acceleration mechanism. For instance if the relic has passed the shock already, the diffusion coefficient directly behind the shock $\kappa_{2,\text{shock}}$ differs from that within the relic $\kappa_{2,\text{relic}}$, and the ratio $\kappa_{2,\text{relic}}/\kappa_{2,\text{shock}}$ would enter Eqs. 12 and 13.

The ratio between break and cutoff momentum of 1253+275

$$\zeta = \frac{p_{\text{break}}}{p_{\text{cut}}} = \frac{F}{G_2 D} = \frac{\kappa_2}{U_2 D} \left(q \frac{a_2}{a_1} + q - 3 \right) \quad (14)$$

must be smaller than 0.18, since the radio spectrum does not exhibit any break or cutoff over a frequency range of about $1\frac{1}{2}$ orders of magnitude. The term in brackets is in the range 1 – 3 and can be neglected for an order of magnitude estimate of the diffusion coefficient behind the shock:

$$\kappa_2 \approx V_s D \zeta / R < 3 \cdot 10^{30} h_{50} \text{ cm}^2 \text{ s}^{-1}. \quad (15)$$

3. Field Compression and Radio Polarization

3.1. General Considerations

The high degree of polarization of relic sources should result from the compression, which aligns unordered magnetic fields with the shock plane. If the shock processed relic is seen at some angle $\delta > 0^\circ$ between the line-of-sight and the normal of the shock front, the field structure projected onto the plane of sky shows a preferential direction. Thus, the resulting radio polarization depends on δ and R . The direction of the magnetic field should appear to be perpendicular to the line connecting the relic and the cluster center, because of this compression and projection effects. This is the case for 1273+275 (Andernach et al. 1984).

In the following we calculate the magnetic field compression and alignment, and the resulting radio polarization of an unordered magnetized plasma blob in an unmagnetized gas flow going through a shock. The (complex) polarization of synchrotron radiation of an isotropic distribution of electrons within a magnetic field seen from the z -direction is given as (Burn 1966)

$$P = \frac{\gamma + 1}{\gamma + \frac{7}{3}} \frac{B_y^2 - B_x^2 - 2iB_x B_y}{B_y^2 + B_x^2}. \quad (16)$$

The spectral index of the electrons is $\gamma = 2\alpha + 1$, where α is the spectral index of the radio emission. In order to average over regions with different field orientations and strength, we have to take into account the different emissivities

$$\varepsilon_{\text{sync}} = a_{\text{sync}} (B_y^2 + B_x^2)^{\frac{\alpha+1}{2}}. \quad (17)$$

Burn has argued that the case $\alpha = 1$ is a valid simplification, which is justified especially in our case, where $\alpha \approx 1$. Averaging the polarization (denoted by $\langle \dots \rangle$) over a (point symmetric) distribution of fields, weighted with the relative emissivity $\varepsilon_{\text{sync}} / \langle \varepsilon_{\text{sync}} \rangle$, gives the observed integral polarization:

$$\langle P \rangle = \frac{\gamma + 1}{\gamma + \frac{7}{3}} \frac{\langle B_y^2 \rangle - \langle B_x^2 \rangle}{\langle B_y^2 \rangle + \langle B_x^2 \rangle}. \quad (18)$$

A magnetic flux tube with field strength B_1 oriented at some angle θ_1 to the normal of the shock front will be bent and amplified by a compression \tilde{R} . From flux conservation it follows that

$$\tan \theta_2 = \tilde{R} \tan \theta_1 \quad (19)$$

$$B_2 = B_1 \sqrt{\cos^2 \theta_1 + \tilde{R}^2 \sin^2 \theta_1}. \quad (20)$$

Observing this field, which is given by its spherical coordinates $(B_2, \theta_2, \phi_2 = \phi_1)$, at the viewing angle δ results in

$$\begin{pmatrix} B_x \\ B_y \\ B_z \end{pmatrix} = \begin{pmatrix} \cos \delta \cos \phi_2 \sin \theta_2 - \sin \delta \cos \theta_2 \\ \sin \phi_2 \sin \theta_2 \\ \sin \delta \cos \phi_2 \sin \theta_2 + \cos \delta \cos \theta_2 \end{pmatrix} B_2. \quad (21)$$

Eq. 18 can now be integrated, assuming an isotropic distribution of the unshocked fields B_1 and choosing the compression ratio of the fields \tilde{R} , which depends on the shock compression ratio R and the field orientation. We discuss two complementary extreme cases, which give similar polarizations.

3.2. Weak Fields

If the magnetic pressure of the relic is small compared to the internal gas pressure the compression of the magnetized regions is equal to the compression of the accretion shock: $\tilde{R} = R$. The calculation of the integrals of Eq. 18 is straightforward if the ensemble average is done over the isotropic, unshocked fields, transformed via Eqs. 19, 20, and 21 to the shocked fields in the observer's coordinate system:

$$\langle P_{\text{weak}} \rangle = \frac{\gamma + 1}{\gamma + \frac{7}{3}} \frac{\sin^2 \delta}{\frac{2R^2}{R^2-1} - \sin^2 \delta}. \quad (22)$$

Inserting numbers of the relic 1253+275 ($\delta = 37^\circ$, $R = 3.2 \pm 0.2$, and $\gamma = 3.36 \pm 0.122$, derived from $\alpha = 1.18 \pm 0.06$) gives a polarization of $\langle P_{\text{weak}} \rangle = 15\%$. The observed polarization of $P_{\text{obs}} = 25\% - 30\%$ (Giovannini et al. 1991) is higher and might indicate an intrinsically ordered field structure of the relic as could be left behind from ordered field structures within an unshocked radio lobe or tail as a progenitor. Or it is due to a larger viewing angle of $\delta = 48^\circ - 52^\circ$, corresponding to an accretion shock radius of $r_s = 4.0 - 3.6 h_{50}^{-1}$ Mpc instead of

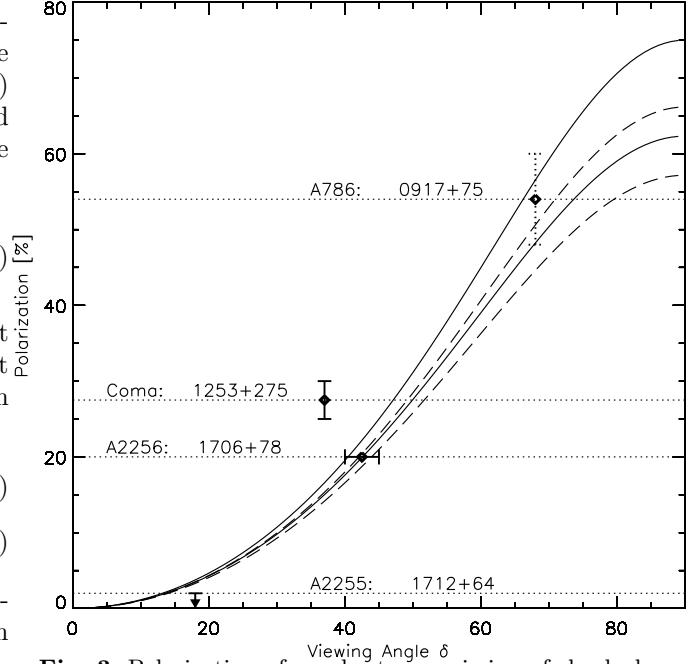


Fig. 3. Polarization of synchrotron emission of shocked magnetic fields as a function of the viewing angle δ . The strong field case is given by solid lines, the weak field case by dashed lines. The upper pair of curves (solid & dashed) corresponds to a radio spectral index of $\alpha = 1$, and therefore $\gamma = 3$ and $R = 4$. The lower lines correspond to $\alpha = 1.5$, $\gamma = 4$ and $R = 2.5$. Observed polarizations of radio relics are plotted above the viewing angle predicted from the accretion shock theory (1253+257, 1712+64), simulations of a cluster merger (1706+78), or – if no data is available – at their best-fit position (0917+75). The large projected radius of 0917+75 indicates a large viewing angle, consistent with the best-fit position. Uncertainties in the angles are large.

$r_s = 4.8 h_{50}^{-1}$ Mpc, as given by Eq. 1. Regarding all the simplifying assumptions made to derive both estimates (Eqs. 1 and 22) of the shock radius, especially the assumed spherical symmetry, we feel that the derived values are quite consistent.

3.3. Strong Fields

If the relic is supported by magnetic pressure only, then the compression of flux tubes differs from the compression of the unmagnetized surrounding medium: The progenitor of the cluster relic, an extended radio lobe, was in pressure equilibrium with its surrounding gas in the upstream region. After the radio plasma has passed the shock, it expands or contracts rapidly, depending on the field orientation, in order to achieve pressure equilibrium with its environment again, since the downstream flow (in the rest frame of the shock) is subsonic. This relates the upstream and downstream fields by $B_2^2/B_1^2 = P_2/P_1$. Eqs. 4 and 20

then give the field compression factor as a function of the field orientation:

$$\tilde{R}(R, \theta_1) = \sqrt{\frac{\frac{4R-1}{4-R} - \cos^2 \theta_1}{\sin^2 \theta_1}} \quad (23)$$

The polarization in the strong field case is then

$$\langle P_{\text{strong}} \rangle = \frac{\gamma + 1}{\gamma + \frac{7}{3}} \frac{\sin^2 \delta}{\frac{2}{15} \frac{13R-7}{R-1} - \sin^2 \delta} . \quad (24)$$

Inserting the numbers of 1253+275 gives $\langle P_{\text{strong}} \rangle = 16\%$. This is similar to the weak field case, also demonstrated by Fig. 3. Magnetic fields of $1.9 h_{50}^{-1/4} \mu\text{G}$ are necessary within 1253+275 in order to support this structure against the thermal pressure at a cluster radius of $4.8 h_{50}^{-1} \text{Mpc}$, assuming a density and temperature as given in Sect. 2.2 and a magnetic pressure of $B^2/(8\pi)$. This rough estimate depends on an extrapolation of the central density profile of the cluster, and has therefore a large error. The magnetic field strength could be lower if nonmagnetic pressure such as thermal gas and/or relativistic particles also support the radio structure. This number is higher than the magnetic field strength derived from minimum energy arguments of the synchrotron emitting plasma of $0.5 h_{50}^{2/7} \mu\text{G}$ measured by Giovannini et al. (1991). Since these authors use a source depth of $400 h_{50}^{-1} \text{kpc}$ along the line-of-sight, while we expect only $125 h_{50}^{-1} \text{kpc}$ due to the compression of the source by the shock, we can correct this number for our model to $0.7 h_{50}^{2/7} \mu\text{G}$. Using the rise of the thermal and (here in the strong field case) of the magnetic pressure given by Eq. 4 we find that the field strength of the unshocked relic plasma needs to be $0.18 \mu\text{G}$, if the equipartition value gives the relic field strength, or $0.5 \mu\text{G}$ if only magnetic pressure has to support the relic. Field strengths of the pre- and after-shock region should be within these ranges.

3.4. Depolarization

A somewhat stronger difference between the polarization in the strong and weak field case might arise from internal Faraday depolarization, which should only appear in the weak field case, since the relic has to be filled with a sufficient amount of thermal gas. Internal depolarization should be strongest for large viewing angle δ , due to the larger number of field lines aligned with the line-of-sight.

We believe that the strong field case is a better description of the remnant of a radio galaxy's lobe, since we find rough equivalence between the measured equipartition field strength and predicted magnetic fields from pressure equilibrium with the surrounding gas. Therefore, internal depolarization should be weak. We do not attempt any estimate because of the large uncertainties entering the calculation such as coherence scale of the fields, the true field strength, and gas density in the relic.

External Faraday depolarization can lower the observed polarization if the relic is seen through the central magnetized regions of the cluster. The degree of depolarization would depend on the field strength and reversal scale within the intra-cluster medium, where both quantities have large uncertainties (Kim et al. 1986; Feretti et al. 1995; Enßlin et al. 1997; Enßlin & Biermann 1997). In order for external depolarization to occur the relic has to be on the back side of the cluster, and its viewing angle δ must be low. Since then the polarization of the relic would be very small anyway, we do not need to correct for this.

We note that, since the observed polarization of 1275+273 is high, nearly all of the synchrotron emission has to come from the ordered fields of the post-shock region as assumed in Sect. 2.4, otherwise the polarization would be lower.

4. X-Ray Emission from Inverse Compton Scattering

The same electrons that emit the synchrotron radiation of the relic should inverse-Compton scatter microwave background photons to the X-ray range. Goldschmidt & Rephaeli (1994) calculated the flux from 1253+275 to be:

$$F_X(\varepsilon_\gamma) = \frac{7.1 \cdot 10^{-5}}{\text{cm}^2 \text{s keV}} \left(\frac{\varepsilon_\gamma}{\text{keV}} \right)^{-2.18} \left(\frac{B_2}{\mu\text{G}} \right)^{-2.18} . \quad (25)$$

Since only a very low thermal X-ray background is produced at such a large cluster radius, this inverse-Compton flux should be best detectable at keV energies. The predicted flux in the ROSAT 0.5-2.4 keV band is $F_{X,0.5-2.4\text{keV}} = 1.2 \cdot 10^{-4} (B_2/\mu\text{G})^{-2.18} \text{cm}^{-2} \text{s}^{-1}$. The observed X-ray energy flux from the Coma cluster is plotted in Fig. 2 of White et al. (1993), and is $9 \cdot 10^{-12} \text{erg cm}^{-2} \text{s}^{-1} \text{deg}^{-2}$ at the position of the relic (assuming a emission temperature of 8 keV). This can be translated into an observed flux of $F_{X,0.5-2.4\text{keV}} = 4 \cdot 10^{-4} \text{cm}^{-2} \text{s}^{-1}$ coming from the field covered by the relic. Comparing this number with the predicted flux implies a field strength of $B_2 > 0.6 \mu\text{G}$, since most of the observed X-ray emission should belong to the X-ray blob centered on NGC 4839. This field strength is in good agreement with the field strength derived by minimum energy arguments and pressure equilibrium, given in Sect. 3.3. It has to be noted though that if a break in the synchrotron spectrum below the observed range (150 MHz – 4.75 GHz) indicates a break in the relativistic electron population, the resulting inverse-Compton flux in the ROSAT band would be largely reduced, since radio frequency ν translates into inverse Compton energy via $\varepsilon_\gamma = 1 \text{keV} (B_2/\mu\text{G})^{-1} (\nu/10 \text{MHz})$ in the monochromatic approximation of the synchrotron and inverse Compton formulae (Blumenthal & Gould 1970). Assuming a break in the radio spectral index of 0.5 at 10 MHz or 100 MHz

still gives lower limits of $B_2 > 0.4 \mu\text{G}$ or $> 0.2 \mu\text{G}$, respectively. The latter value can be regarded as a hard lower limit to the relic field strength.

1253+275 should be an interesting object for future X-ray telescopes, such as XMM and AXAF, because its large-scale inverse Compton flux might be detected, or stronger limits to the magnetic fields and/or the low-energy electron spectrum can be derived. The radio halo of the Coma cluster should have a larger inverse-Compton flux, but there the keV range is polluted by thermal emission and has to be avoided by using other energy bands (Rephaeli et al. 1994, Enßlin & Biermann 1997).

5. The Origin of Relics

5.1. Radio Galaxies

Relics are believed to be remnants of former radio galaxies. The problem that the energy loss time scale is frequently shorter than the time elapsed since the last resupply with energetic electrons from a progenitor radio galaxy is solved in our approach due to the acceleration by the large-scale accretion shocks. Therefore the progenitor radio galaxy needs not to be within the distance from the relic a galaxy can travel with a typical cluster velocity within a cooling time of the electrons. In order to explain the polarization by field compression, it is necessary though that the radio plasma from which the present day radio emission results was injected within the upstream region. The large spatial extent of relics might result from the much lower pressure in the upstream regions, so that the radio lobes could expand over a larger volume than a similar radio galaxy would have occupied in the intra-cluster medium inside the accretion shock.

It is interesting to remember that the minimum magnetic pressure of 1253+275 is near equipartition with the expected thermal pressure at the shock radius (estimated using an extrapolation of the central density profile), whereas minimum pressures of radio lobes of active radio galaxies in the interior of galaxy clusters usually are much lower than the gas pressure at their radii, even if projection effects are taken into account (Feretti et al. 1992). Several effects can explain this latter pressure imbalance, despite the possibility that minimum energies do not describe the physical conditions:

- a filling factor of the observed radio plasma of a few percent
- the ubiquitous presence of relativistic protons within the lobes, dominating the energy density of relativistic particles
- the existence of a significant number of low-energy electrons radiating below the adopted low-frequency cutoff of the minimum energy analysis
- a significant amount of thermal gas within the lobes.

Under the hypothesis that relics are old lobes, the filling factor and also the low-energy electron population should

be similar in both types of sources, and therefore not responsible for differences of cluster relics and lobes in the central regions of clusters. Thermal gas remains to be the explanation, and also relativistic protons, because the possible rich initial proton population of the lobes might be escaped due to the larger age and the higher cosmic ray diffusion coefficient of relics compared to lobes inside clusters.

Giovannini et al. (1985) propose the Coma cluster galaxy IC 3900 to be the origin of 1253+275, which should have moved to another position on the plane of the sky. We point out that the narrow-angle tail (NAT) radio galaxy NGC 4789 is a very attractive possible origin, too. First, a bridge of radio emission connects it with the central ridge of the relic (Giovannini et al. 1991), indicating a geometrical connection. Second, 1253+275 lies on the (projected) line between NGC 4789 and the center of the Coma cluster. NGC 4789 is therefore an ideal candidate for being the source of magnetized plasma injected upstream into the accretion flow. The NAT structure of NGC 4789 might result from the ram-pressure of the infalling matter on the radio jets, enhanced by an ascending movement of the galaxy. Relativistic electrons from the jets should be convected by the flow within the radio bridge to the accretion shock, where they are reaccelerated and radiate. The line-of-sight velocity of NGC 4789 is higher by 1179 km s^{-1} than Coma's Hubble velocity (Venturi et al. 1988). This implies, if NGC 4789 is really located upstream above 1253+275, that we see a relic on the back side of the accretion shock sphere. This is sketched in Fig. 2. If NGC 4789 is on a radial ascending orbit, its velocity should be 1480 km/s (assuming $\delta = 37^\circ$), similar to that of the infalling matter measured in the clusters rest frame $\tilde{V}_s = 1400 \text{ km/s}$. The radio plasma, which is reaching the shock today, was thus injected into the stream half a Gyr ago, given that its movement is only due to convection by the accretion flow.

5.2. Large-Scale Fields

A very different nature of the origin of the magnetic fields in the relic is imaginable: from simulations of magnetic field generation and amplification by turbulence in the flows of large-scale structure formation field strengths of the $0.1 \mu\text{G}$ level within cosmological filaments are predicted by Biermann et al. (1997). The predicted field strengths at cluster accretion shocks are $B_2 \approx \mu\text{G}$, being in energetic equipartition with the thermal energy density. In the inner regions of clusters, field strengths at the $10 \mu\text{G}$ level are expected, as Enßlin et al. (1997) argue to be injected from radio galaxies, presuming that their jets also contain energetic protons. If field values of $B_2 \approx \mu\text{G}$ are typical for the accretion shock region, it has to be explained what is special at the positions of relic sources. In the case of 1273+275 this should be the presence of NGC 4789 providing preaccelerated electrons injected into the

accretion flow, efficiently reaccelerated at the shock front below the galaxy.

It is remarkable that the 1253+275 complex is in the elongation of the Coma cluster, which itself appears to align with Coma/Abell 1367 filament of galaxies as described by Fontanelli (1984). It is possible that the position of the relic traces the working surface of a large-scale stream flowing out of this filament and hitting the sea of cluster gas. The observed radio bridge connecting 1253+275 and the radio halo Coma C (Kim et al. 1989) then might be a deposition of magnetic fields from this stream, illuminated by relativistic electrons accelerated in the shock.

6. Other Relics

6.1. General Remarks

A handful of other cluster relics are known. Their properties and that of their host clusters are collected in the upper part of Tab. 1. According to the theory discussed in this paper other quantities are calculated and given in the lower part of Tab. 1. Average values for 1253+275 are also given in Tab. 1, but the very recently discovered relic 2010-57 (Röttgering et al 1997) is only discussed in the text.

For four relics, namely 0917+75, 1253+27, 1712+64, and 1706+78, polarization measurements are available. In three cases these polarizations fit well into the prediction of the accretion shock theory (see Fig. 3). In the case of 1706+78 in A2256 the observed polarization is much higher than expected. This can be understood if the shock is due to an on-going merger event (Fabian & Daines 1991), and therefore located at a smaller cluster radius. The accretion shock theory predicts a polarization of 28% for the relic 2006-56, 10% for 2010-57, 4% for 1140+203 and 1401-33, and 1% for 0038-096.

The predicted shock velocity $V_{s,\text{predicted}}$ is in all accretion shock examples lower than that of the accretion shock theory of Kang et al. (1997) by 16% on average. This could be due to an assumed temperature drop of a factor of less than two from the cluster center to the accretion shock radius, or due to the need of some recalibration of the accretion shock parameters.

Looking at the distribution of the predicted viewing angle δ one recognizes that large angles are underrepresented. In an isotropic distribution half of the relics should be seen at a viewing angle above 60° . This is clearly a selection effect, since the sensitive radio surveys of clusters with good angular resolution which are needed for the detection of these sources, usually do not reach projected radii of 5 Mpc, as would be necessary in order to include the whole accretion shock. We expect therefore that undiscovered relics, with strong radio polarizations, are waiting in these outer regions of clusters for their exploration.

6.2. Abell 85: 0038-096

The spectral index of 0038-096 is not settled in the literature: Slee & Siegman (1983) give $\alpha = 1.60$, Reynolds (1986) gives $\alpha = 2.90$, Slee et al. (1994) 2.37, Joshi et al. (1986) 3.03 above a break at 300 MHz, whereas Ferretti & Giovannini (1996) state that $\alpha > 1.5$. We base our estimates mainly on the numbers of the latter authors. It is possible that the observed strong steepening is in fact a smeared-out cutoff, resulting from the limited acceleration power of a weak accretion shock. Since the projected relic position is close to the cluster center the viewing angle is close to zero and therefore no visible polarization resulting from field compression is expected. The necessary radio efficiency η_{radio} of the shock is $> 1\%$ and thus reasonable. The predicted magnetic field strength $B_{2,\text{predicted}} = 2.6 \mu\text{G} h_{50}^{-1/4}$ from assuming pressure equilibrium between the post-shock gas and the relic is again higher than the equipartition (or minimum energy) value given by Ferretti & Giovannini (1996) $B_{2,\text{eq}} < 1.4 \mu\text{G} h_{50}^{2/7}$ (corrected by $R^{2/7}$). Lima Neto et al. (1997) report the appearance of an X-ray blob in the X-ray image of A85 centered on 0038-096, possibly inverse-Compton scattered microwave background photons. If so, the magnetic field strength could be derived directly from an estimate of this X-ray excess.

6.3. Abell 786: 0917+75

The megaparsec cluster radio relic 0917+75 is located 5 Mpc h_{50}^{-1} away from the center of A786 within the plane of sky. Unfortunately no temperature or velocity dispersion of A786 is available in the literature. Thus, the expected shock radius and therefore the polarization cannot be predicted. However the very peripheral position indicates a large viewing angle, consistent with the high degree of the observed polarization of 48 – 60%. A viewing angle of $72^\circ - 63^\circ$ corresponding to an accretion shock radius of $5.6 - 5.3 \text{ Mpc } h_{50}^{-1}$ would be in agreement with this polarization. Such a large shock radius indicates a deep gravitational potential. The corresponding virial temperature 13 – 15 keV (Eq. 1) is in the upper range of observed temperatures of clusters, and therefore possible. However the shock structure might in fact be also due to an accretion flow, which is centered on and stops at the boundary of the supercluster Rood #27, which A786 is a member of. This could explain the large projected shock radius.

The direction of the projected magnetic field observed by radio polarization is mainly perpendicular to the axis connecting the center of A786 and 0917+75, as it should be if the field is compressed at a spherical shock centered on the cluster. But a weakly visible spiral structure in the projected fields could result from an intrinsic order which the magnetic fields had before they passed the shock.

The relic 0917+75 exhibits a break in its spectrum (Harris et al. 1993). Below 300 MHz the spectral index

Cluster Relic		References	A85 0038-096	A786 0917+75	A1367 1140+203	Coma 1253+275	A2255 1712+64	A2256 1706+78	A3667 2006-56	S753 1401-33
z		fovfffn	0.0559	0.125	0.0216	0.0233	0.0824	0.0824	0.0566	0.0142
kT_{obs}	keV	e-dbdrf	6.2	—	3.7	8.2	7.3	7.3	6.3	2.5 ⁽⁶⁾
$n_{e,o}$	$10^{-3} \text{ cm}^{-3} h_{50}^{1/2}$	p-pbhpr-	5.5	—	0.95	3	1.8	2.5	1	—
r_{core}	kpc h_{50}^{-1}	p-pbhar-	225	—	430	400	579	352	286	—
β		e-pbhar-	0.62	—	0.52	0.75	0.74	0.76	0.54	—
$r_{\text{projected}}$	Mpc h_{50}^{-1}	soilhtmn	0.64	5	1.09	2.9	1.25	0.74	2.95	0.911
α		gojlhtun	>1.5 ⁽¹⁾	1.1	1.9	1.18	1.4	0.8 ⁽²⁾	1.1	1.4
P	%	-ol-ht-	—	54	—	27	<2	20	—	—
$B_{2,\text{eq}}$	$\mu\text{G } h_{50}^{2/7}$	gojlhtmn	<1.4	0.5	2	0.7	0.6	2.7	1.6	0.4
D	Mpc h_{50}^{-1}	soilhtmn	>0.096	0.22	0.088	0.1	0.075	0.1	0.15 ⁽⁵⁾	0.082
S	Mpc ² h_{50}^{-2}	soklhtun	0.096	0.96	0.053	0.48	0.19	0.3	1.8 ⁽⁵⁾	0.11
ν_{break}	MHz	qqjlhtmn	≤300	300	<610	<151	<333	>1500	<85	<843
ζ		qqjlh-mn	<0.45	<0.45	<0.66	<0.18	<0.47	— ⁽²⁾	<0.13	<0.75
$\log(Q_{\text{radio}})$	erg/s h_{50}^{-2}	gojlctun	41.2	41.6	41.5	40.9	40.8	41.5	42.4	41
r_s	Mpc h_{50}^{-1}	Eq. 1	4	—	3.2	4.8	4.1	1.1 ⁽³⁾	4	2.6
V_s	km/s	Eq. 2	1770	—	1370	2040	1920	3000 ⁽³⁾	1780	1120
δ	°	Sect. 2.2	9.3°	—	20°	37°	18°	42° ⁽³⁾	48°	20°
R		Eq. 3	<2.5	3.5	2.1	3.2	2.7	2.9 ⁽²⁾	3.5	2.7
P_2/P_1		Eq. 4	<6	26	3.8	15	7.3	9.3 ⁽²⁾	26	7.3
T_2/T_1		Eq. 4	<2.4	7.4	1.8	4.6	2.7	1.9 ⁽²⁾	7.4	2.7
$n_{e,1}$	$10^{-5} \text{ cm}^{-3} h_{50}^{1/2}$	Sect. 2.3	>1.1	—	1.9	0.35	0.82	6.2	0.42	—
kT_1	keV	Eq. 4	>1.3	—	1	0.88	1.3	3.8 ⁽⁴⁾	0.42	0.45
$V_{s,\text{predicted}}$	km/s	Eq. 5	1440	—	1020	1850	1600	3050	1690	932
$B_{2,\text{predicted}}$	$\mu\text{G } h_{50}^{1/4}$	Sect. 3.3	2.6	—	2.4	1.9	2.5	10	1.9	—
$B_{1,\text{eq}}$	$\mu\text{G } h_{50}^{2/7}$	Sect. 3.3	>0.57	0.098	1	0.18	0.22	0.89	0.31	0.15
$B_{1,\text{predicted}}$	$\mu\text{G } h_{50}^{1/4}$	Sect. 3.3	>1.1	—	1.2	0.5	0.94	3.3	0.38	—
$\log(Q_{\text{flow}})$	erg/s $h_{50}^{-3/2}$	Eq. 6	<43.2	—	42.7	43.7	43.5	45.2	44.2	—
η_{radio}	% $h_{50}^{-1/2}$	Sect. 2.3	>0.99	—	6	0.15	0.18	0.017	1.3	—
$t_{\text{age,kin}}$	$10^8 \text{ year } h_{50}^{-1}$	Sect. 2.4	1.3	—	1.3	1.5	1	0.98	2.9	1.9
$t_{\text{age,break}}$	10^8 year	Eq. 13	≥3.2	1.7	>2.6	>4	>2	<1.4	>6.2	>1.4
$\log(\kappa_2)$	$\text{cm}^2/\text{s } h_{50}$	Eq. 15	<31	<31.4	<31.1	<30.5	<30.9	— ⁽²⁾	<30.5	<30.9
P_{strong}	%	Eq. 24	0.92	—	4	16	3.4	20	28	4.4
δ_{strong}	°	Sect. 3.3	—	68°	—	48°	<14°	43°	—	—
$r_{s,\text{strong}}$	Mpc h_{50}^{-1}	Sect. 3.3	—	5.4	—	3.9	>5.3	1.1	—	—

Table 1. The upper part of the table is a collection of measurements of properties of cluster radio relics and their host clusters. The references are indicated in the third column in the sequence of the eight examples. The lower part gives estimates, using the above properties and the formulae of this paper, as indicated in the third column. A discussion of the individual sources and various assumptions made in order to get the given values can be found in Sect. 6.

Observed Quantities: z : redshift of the cluster. kT_{obs} : observed central gas temperature. $n_{e,o}$, r_{core} , β : parameters of the β -model, describing the radial electron density profile of the cluster $n_e = n_{e,o} [1 + (r/r_{\text{core}})^2]^{-3\beta/2}$. $r_{\text{projected}}$: radius of the position of relic, projected into the plane of sky. α : spectral index of relic's radio emission. P : average observed polarization. $B_{2,\text{eq}}$: equipartition field strength of the relic, the index 2 refers to the post-shock region, where to the visible part of the relic belongs. The values of the literature are changed due to the effect of a smaller volume than assumed there according to $B_{2,\text{eq}} \sim R^{2/7}$, where R is the compression ratio. D : thickness, roughly estimated by dividing the observed projected thickness by the compression R . S : surface area of the relic. Since in all except one cases the relic structure can not be deprojected, we use the observed projected surface as a rough estimate. ν_{break} : break frequency of relic's radio spectrum. ζ : ratio of break- to cutoff momentum of the electron population, estimated from the ratio of break- and cutoff frequency of the radio spectrum by taking the square root. Q_{radio} : relic's radio power, usually assuming a single power law between 10 MHz and 10 GHz.

Estimated Quantities: r_s : shock radius. V_s : shock velocity. δ : viewing angle given by the estimate of the shock radius r_s and the projected radius of the relic r_{proj} . R : shock compression ratio, estimated from the spectral index. P_2/P_1 , T_2/T_1 : pressure and temperature jump across the shock. $n_{e,1}$: upstream side electron density, derived from the β -profile and the compression ratio. kT_1 : temperature of the infalling gas, derived from the post-shock temperature kT_2 , which is assumed to be half of the central temperature kT_{obs} (see Sect. 2.2). $V_{s,\text{predicted}}$: shock velocity, predicted from the post-shock temperature and the compression ratio. $B_{1,\text{predicted}}$, $B_{2,\text{predicted}}$: up- and downstream field strength which would be in pressure equilibrium with the surrounding gas. $B_{1,\text{eq}}$: strength of the magnetic field of the progenitor of the relic source, if the magnetic pressure was increased by P_2/P_1 to $B_{2,\text{eq}}$ in the shock. Q_{flow} : kinetic power of the flow onto the surface of the relic. η_{radio} : radio efficiency $Q_{\text{radio}}/Q_{\text{flow}}$. $t_{\text{age,kin}}$: age of the relic being behind the shock from D/U_2 , where $U_2 = V_s/R$ is the post-shock velocity. $t_{\text{age,break}}$: age of the relic being behind the shock from D/U_2 , where this ratio is derived from the radio break frequency. κ_2 : diffusion coefficient of the post-shock region. P_{strong} : polarization expected in the strong field case, for a viewing angle δ . δ_{strong} , $r_{s,\text{strong}}$: viewing angle and the shock radius computed to be consistent with the observed polarization P .

Remarks:

⁽¹⁾ The lower limit to the spectral index translates into limits of dependent quantities. But the measured steep spectral index might also be due to the appearance of the high frequency cutoff, so that these limits become estimates. ⁽²⁾ A spectral index smaller than unity indicates, that the range observed in the radio is below the break frequency. The spectral index above the break is steeper by 0.5. A after-break spectral index of $\alpha = 1.3$ was used in these formulae. No lower limit to the ratio ζ between cut and break frequency and therefore no diffusion coefficient can be estimated in this case. ⁽³⁾ The results of the accretion shock theory are $r_s = 4.9 \text{ Mpc } h_{50}^{-1}$, $V_s = 2280 \text{ km/s}$, and $P_{\text{strong}} = 0.78\%$. The latter is excluded by the observed polarization of $P = 20\%$. The accretion shock model therefore fails; but as discussed in Sect. 6.6 the shock should result from a merger. We therefore inserted the best-fit numbers from a hydrodynamic simulation of such an event. r_s is set to $r_{s,\text{strong}}$, V_s and δ are taken from Roettiger et al. (1995). ⁽⁴⁾ Since this shock is in the interior of the cluster, $kT_2 = kT_{\text{obs}}$ was used. ⁽⁵⁾ For this relic a deprojection of the geometry was possible as described in the text, and we therefore use these values. ⁽⁶⁾ The velocity dispersion given in Fadda et al. (1996) is translated into a temperature with the help of the dispersion-temperature relation given in Bird et al. (1995).

References: a: Briel et al. (1991), b: Briel et al. (1992), c: Burns et al. (1995), d: David et al. (1993), e: David et al. (1995), f: Fadda et al. (1996), g: Feretti & Giovannini (1996), h: Feretti et al. (1997), i: Gavazzi (1978), j: Gavazzi & Trinchieri (1983), k: Gavazzi & Jaffe (1987), l: Giovannini et al. (1991), m: Goss et al. (1982), n: Goss et al. (1987), o: Harris et al. (1993), p: Jones & Forman (1984), q: Joshi et al. (1986), r: Knopp et al. (1996), s: Lima Neto et al. (1997), t: Röttgering et al. (1994), u: Röttgering et al. (1997), v: Zabludoff (1993)

is 0.6 and above it is steeper by the canonical value 0.5, as is expected from a steepening of the spectral index of the electron population by 1, predicted in Sect. 2.4. The corresponding compression ratio of $R = 3.5$ is close to the maximum possible value $R = 4$ of a strong nonrelativistic shock.

The projected peripheral position of 0917+75 allows a sensitive search for inverse-Compton scattered microwave background photons in the X-ray range. Harris et al. (1995) observed the relic with the PSPC instrument on the ROSAT satellite and got an upper limit to the flux in the 0.5-2.0 keV band of $2.3 \cdot 10^{-14} \text{ erg cm}^{-2} \text{ s}^{-1}$. This implies that the magnetic field strength must be $B_2 \geq 0.8 \mu\text{G}$, slightly larger than $B_{2,\text{eq}} = 0.5 \mu\text{G } h_{50}^{2/7}$ derived from minimum energy considerations and various assumptions, which were discussed in Harris et al. (1995) and Sect. 5.1 of this article.

6.4. Abell 1367: 1140+203

The diffuse radio source found in A1367 is usually called a halo, but it is more probably a cluster relic because of its noncentral location and asymmetric shape. The distance to the center of the galaxy distribution is $0.8 \text{ Mpc } h_{50}^{-1}$ (Gavazzi 1978), but to that of the X-ray emission it is $1.1 \text{ Mpc } h_{50}^{-1}$ (see map in Gavazzi et al. 1995). We use the

latter distance, since the X-ray emission should be a better tracer of the gravitational potential. The X-ray emission is elongated into the direction of the relic, possibly tracing the influence of the large-scale structure potential, or the main direction of the accretion flow onto the cluster, or both. The radio relic could be contaminated or related to three close irregular galaxies, which have radio trails behind them (Gavazzi & Jaffe 1987), indicating that they are falling inwards. Strong on-going star formation, a recent supernova in one of them, and young and abundant H II regions, which are aligned as if they were formed by bow shocks (Gavazzi et al. 1995), could be triggered by the sudden change of the environment of these galaxies during the passage of the accretion shock. A starburst might increase the accretion within these galaxies onto a possible central black hole (similar to the argumentation of Wang & Biermann 1998) and therefore can trigger the ejection of radio plasma.

The measurements of the spectral index and radio flux of the relic differ in the literature (compare Gavazzi 1987, Hanisch 1980, and Gavazzi & Trinchieri 1983) and therefore any derived numbers have to be used with care. Especially the radio power Q_{radio} is an extrapolation of a very steep spectrum ($\alpha = 1.9$) down to 10 MHz and probably an overestimate. Due to the low expected viewing angle only a small polarization of 4% is expected. Gavazzi

& Trinchieri (1983) detected some X-ray emission from the region of the relic. Assuming this to result from inverse Compton emission they estimate a magnetic field strength of $1.2 \mu\text{G}$, of the same order as the equipartition value of $B_{2,\text{eq}} = 2 \mu\text{G} h_{50}^{2/7}$ and the predicted strength of $B_{2,\text{predicted}} = 2.4 \mu\text{G} h_{50}^{1/4}$ for pressure equilibrium with the surrounding.

6.5. Abell 2255: 1712+64

The cluster A2255 has a number of similarities to the Coma cluster: there is evidence that the cluster is in a state of merging (Burns et al. 1995), a radio halo is present, and also a peripheral radio relic without any obvious parent galaxy (Feretti et al. 1997). The spectral index of the relic is fairly constant along the structure. The upper limits to the polarization of 9% at 20 cm and 2% at 90 cm do not contradict the predicted polarization of 3% seriously, taking into account e.g. the rough assumptions which entered the estimate of the shock radius, and the possibility that external Faraday depolarization has lowered the degree of the radio polarization if the relic is seen through the denser magnetized central intra-cluster medium. This relic therefore fits also well into the accretion shock theory.

6.6. Abell 2256: 1706+78

The radio emission reveals a very complex situation within A2256: a mini-halo is visible in the map of Bridle & Fomalont (1976), and several head-tail radio galaxies can be found. One NAT source (in the notation of Bridle & Fomalont (1976): source C) is one of the longest head-tail sources known. The tail extends over $700 \text{ kpc} h_{50}^{-1}$, is slightly bent and exhibits a kink $570 \text{ kpc} h_{50}^{-1}$ behind the head (Röttgering 1994). The bending can be understood as the gravitational influence of the cluster mass to the trajectory of a fast radio moving radio galaxy, at which the tail traces the path. The kink might result from a sudden change of the surrounding density or velocity field of the background gas (Röttgering et al. 1994), as it might happen if the radio galaxy passes a shock. The projected position of the kink is within a very extended irregular and sharp-edged region of diffuse radio emission in the north-west region of the cluster. This region consists of two extended sources (G and H in the notation of Bridle & Fomalont (1976)), which might be two independent relic sources with similar properties.

The spectral index of 0.8 of these possible cluster relics indicates that the injection electron spectrum below the break in the momentum distribution are observed. The spectral index of the synchrotron emission above the break should be $\alpha = 1.3$. The break momentum (Eq. 12) is highest for a large shock velocity V_s and a thin magnetized post-shock region (small D). The latter could explain why the emission region is relatively sharp-edged. If the thickness D is much smaller than we assumed, the

kinematic age of the relic $t_{\text{age,kin}}$ would be much smaller than 10^8 yr , in accordance with $t_{\text{age,break}} < 1.4 \cdot 10^8 \text{ yr}$. The polarization of 20% is much too high for the expected viewing angle $\delta = 9^\circ$ of a relic located at the canonical radius of the accretion shock $r_s = 5 \text{ Mpc} h_{50}^{-1}$, which predicts only 1% polarization. A consistent viewing angle of $\delta_{\text{strong}} = 43^\circ$ would imply that if the normal of the shock front is pointing to the cluster center, the shock radius is $r_s = 1 \text{ Mpc} h_{50}^{-1}$. This would be in agreement with the average direction of the polarization, which is oriented roughly perpendicular to this assumed normal of the shock front. A shock in the interior of the cluster can only be explained by a merger event. Independent evidence for such a collision can be found in the X-ray morphology, in the complex temperature structure and in the elongated galaxy distribution. An extensive discussion of the observational signs reported in the literature is given by Roettiger et al. (1995). They compare these observations with simulations of cluster mergers and conclude that the entire data are best reproduced by a merger of two clusters with mass ratio 1:2 and a relative velocity of 3000 km/s . The separation of the cluster centers is $0.75 \text{ Mpc} h_{50}^{-1}$. The smaller cluster is infalling from the north-west and is approaching the observer. The angle between the line-of-sight and the merger axis is in the best-fit model in the range of 40° to 45° , in agreement with $\delta_{\text{strong}} = 43^\circ$ estimated from polarization, without taking any possible influence of external Faraday depolarization into account.

The temperature kT_{obs} given in Tab. 1 is an average value of a complex distribution, biased by the heat production of the shock. Since the infalling subcluster has a much higher temperature ($kT_1 \approx 4 \text{ keV}$; $kT_2 = kT_{\text{obs}}$ is assumed here) than the accretion streams hitting all other known cluster relics ($kT_1 \approx 1 \text{ keV}$), the moderate shock compression ratio $R = 2.9$ at this shock, which has the highest shock velocity of our sample, can be understood to result from the high pressure of the upstream matter.

The predicted shock velocity derived from the upstream temperature and pressure jump is $V_{s,\text{predicted}} = 3050 \text{ km/s}$, being in agreement, and completely independent of the above mentioned merger velocity from the hydrodynamic simulations. The merger velocity corresponds to the infall velocity measured in the cluster rest frame \tilde{V}_s , which is usually lower by $(R - 1)/R$ than the shock velocity V_s . But in case of a massive merger it is unrealistic to believe that A2256 behaves like a single body, the downstream flow does surely not rest in the cluster reference frame. We therefore use a realistic velocity of $V_s = \tilde{V}_s = 3000 \text{ km/s}$.

The line-of-sight velocities of the head-tail radio galaxies also point towards the observer, and especially the obviously fast moving source C seems to originate from the infalling cluster. Röttgering et al. (1994) have fitted trajectories, calculated for a gravitational potential derived from X-ray data to the tail of source C, and concluded that the initial velocity had to be in the range of 2000-3500

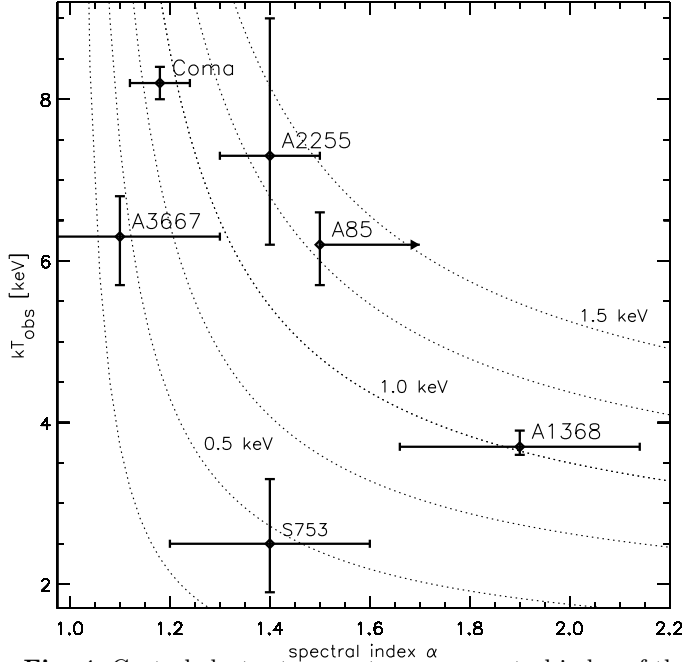


Fig. 4. Central cluster temperatures vs. spectral index of the radio relics. The dotted lines are temperature-spectral index relations, computed from the temperature jump given by Eq. 4, which for a given temperature of the infalling gas kT_1 (and assuming $kT_2 = \frac{1}{2}kT_{\text{obs}}$) is a function of the spectral index α only. The temperature of the infalling gas kT_1 is indicated for the curves.

km/s, in accordance with the value of the relative cluster velocity given by Roettiger et al. (1995). From the undisturbed straightness of the source Röttgering et al. (1994) derive that the turbulent motion of the cluster medium has a velocity < 200 km/s, much too low to explain the diffuse emission resulting from large-scale turbulent motion. However, this is not in contradiction to the merger shock model for this relic, where violent velocity changes occur only in the thin shock region, which might have distorted the tail of source C at the position of the kink. We note, that a brightening of the radio tail is visible there, as expected to result from the action of the shock onto the tail (Röttgering et al. 1994). Source C should have moved from the kink within $2 - 3 \cdot 10^8$ years to its present day position. This is comparable or higher than a typical cooling time of radio emitting electron, and explains the observed fading of the tail.

The details of the complex scenario might differ from the above picture in that the shock might be oblique (Roettiger et al. 1995), or the impact parameter of the merging clusters is non-zero (Briel et al. 1991).

6.7. Abell 3667: 2006-56 and 2010-57

The giant cluster radio relic 2006-56 is peripherally located within the direction of the elongation of A3667. This elongation is seen in X-rays, but also contains a subgroup of galaxies (Knopp et al. 1996). Because of the low X-ray

background, 2006-56 would be an ideal candidate for a future sensitive search for inverse Compton flux (by, e.g., AXAF, XMM). Goss et al. (1982) separated two extended radio sources at this position, located close to each other: 2006-56 and a diffuse ridge. A recent sensitive observation by Röttgering et al. (1997) shows that there is in fact a single Z-shaped structure, extending over $2.6 \text{ Mpc } h_{50}^{-1}$, with constant spectral index along the main axis of the relic. The Z-shape might be the structure of the radio plasma, since we do not see the relic edge-on. The side more distant from the cluster center is sharply edged and has a flatter spectral index, as is expected to happen on the upstream side as explained in Sect. 2.1. The spectral index drops from $\alpha = 1.1$ in the central region of the relic to ≈ 0.5 at this edge. This indicates strongly the presence of particle acceleration, so that we can use the thickness of the rim of lower spectral index in order to estimate the thickness of the relic. The projected thickness derived from the rim is approximately $100 - 200 \text{ kpc } h_{50}^{-1}$. The region with steeper spectral index on the inner side has also a projected thickness of $\approx 200 \text{ kpc } h_{50}^{-1}$. Assuming a viewing angle of $\delta = 48^\circ$, deprojection gives $D \approx 150 - 300 \text{ kpc } h_{50}^{-1}$. The projected area of the relic is $1.6 \text{ Mpc}^2 h_{50}^{-2}$. A stripe of $150 \text{ kpc} \times 2.6 \text{ Mpc}$ belongs to one edge. Deprojecting the remaining area gives a relic surface of $1.8 \text{ Mpc}^2 h_{50}^{-2}$. The infalling gas seems to be relatively cool, with $kT_1 \approx 0.4$ keV, but this number has a large error since the temperature jump is very sensitive to small variations in R , since R is close to its maximum value (see Eq. 4 or Fig. 4).

Röttgering et al. (1997) report a pressure imbalance of one to two orders of magnitude, between the gas pressure at the projected cluster radius of the relic and its equipartition pressure. This discrepancy should vanish if the lower gas pressure at the shock radius and the higher radio plasma pressure of a compressed, flattened structure is taken into account. Therefore we find good agreement between equipartition field strength and predicted field strength.

Surprisingly, the radio image of Röttgering et al. (1997) reveals a second cluster radio relic on the other side of the cluster (2010-57). These authors mention that both relics might be the two lobes of a former, now inactive, radio galaxy, possibly the cD galaxy. This must have been gigantic, since the projected distance is $5.2 \text{ Mpc } h_{50}^{-1}$. The expected diameter of the accretion shock sphere of $8 \text{ Mpc } h_{50}^{-1}$ would be a lower limit to the extent of this radio galaxy in our scenario, since nowadays we would see a backflow of the radio lobe from larger distances. In order to achieve such an extent, the radio galaxy must have been very powerful and the ambient medium more tenuous than today. If both structures are really produced by one galaxy, this should have happened during the early period of violent quasar activity, when the intra-cluster medium was thinner.

If the two relics are independent, in the sense that their radio plasma is from different sources, but their po-

sitions are correlated due to the membership of A3667 to a large-scale filament, then the head-tail radio galaxy B2007-569 can be the source of the shocked radio plasma in 2006-56. It is located between the cluster center and the relic and is moving towards us with a speed of 1200 km/s ($z = 0.05257$; Sodré et al. 1992). If it is on a radially falling orbit, which traversed the shock sphere at the location of the present day relic, it should have a velocity of 1800 km/s (using $\delta = 48^\circ$), higher than the expected infall velocity of matter (measured in the cluster rest frame) at the higher radius of the shock. Travelling with this velocity it should have passed the shock a Gyr ago. This is an order of magnitude longer than a typical cooling time of radio emitting electrons and therefore the expected trace of radio plasma on the path of that galaxy became invisible. It is amazing that Röttgering et al. (1997) found marginal evidence for a bridge between this galaxy and the relic, which might indicate reacceleration.

We predict a polarization in 2006-56 of 28% from our accretion shock model, and 10% in 2010-57 due to its smaller expected viewing angle of 30° , assuming the same spectral index and shock compression ratio as for 2006-56. The observation of these polarizations would be an independent test of the theory, and therefore could verify general assumptions made about large-scale flows in the Universe.

6.8. Abell S753: 1401-33

S753 is a poor cluster. Its low velocity dispersion of 536 km/s (Fadda et al. 1996) indicates a low central gas temperature of $kT_{\text{obs}} = 2.5$ keV, applying the dispersion-temperature relation given in Bird et al. (1995), and therefore a flat gravitational potential compared to the other clusters. The spectral index $\alpha = 1.4$ of the relic 1401-33 corresponds to a shock compression ratio of $R = 2.7$. This relatively strong shock at this poor cluster can be understood if the accreting matter has a temperature of $kT_1 \approx 0.5$ keV. This is lower than what seems to be typical for the other clusters ($kT_1 \approx 1$ keV, see Fig. 4). The lower preheating of the flow onto this cluster might indicate a poorer cosmological environment. Since the sky position of the relic 1401-33 is close to the center of S753, the viewing angle should be small and only 4% polarization is predicted.

7. Conclusions

From simulations of the structure formation of the Universe, large accretion shocks around clusters of galaxies are expected. If magnetic fields are present at these locations, particle acceleration should take place. Protons might be accelerated to the highest observed energies, as demonstrated by Kang et al. (1997), because of their weak energy losses and their possible injection out of a thermal population. If a population of relativistic low-energy electrons is

also present, they would be accelerated, too. High-energy ultra-relativistic electrons lose energy by inverse-Compton scattering and synchrotron emission. This allows to see them in the radio or X-ray regime and therefore verify the existence of the large-scale formation shock structures.

At peripheral positions with respect to the cluster center regions of diffuse radio emission are found, the so-called cluster radio relics (Figs. 1 and 2). They are assumed to be remnants of radio galaxies. Their energy supply was a long lasting outstanding problem, since their electron cooling times are usually too short to allow any of the nearby possible former parent galaxies to have moved from the relic to its present position within that time. Electron acceleration has to take place within them, but turbulent acceleration from galactic wakes fails to explain this, due to the low galaxy densities in these regions.

If these relics are close to the accretion shock, a shock efficiency of only 0.1 – 5% is sufficient to power them. The accretion shock itself should collect relics since every volume filled with radio plasma, being injected into the intergalactic medium above such a shock by a radio galaxy, would be dragged into the shock by the fast motion of the infalling gas. After passing the shock, the relic remains close to it for some time, since the growth rate of the shock radius is much slower than the accretion velocity. Buoyant motion of the light radio plasma embedded in the heavier surrounding gas might help to keep it longer there.

The relic is proposed to be radio illuminated by relativistic electrons (re)accelerated at the shock and therefore tracing its position. The radio spectrum of such relics is steeper than expected for electron acceleration within strong shocks, indicating that the temperature of the infalling matter should be $\approx 0.5 - 1$ keV (see Fig. 4). Thus, preheating of this gas should have taken place. The accreting gas has a typical density of $n_{e,1} \approx 10^{-5} \text{ cm}^{-3} h_{50}^{1/2}$. 1706+78 in A2256 of course does not fit into this temperature scheme, due to its different physical nature, being located at a merger shock front in the interior of the cluster. Matter which has fallen onto the large-scale cosmic sheets should be shock-heated to about 0.1 keV and have a density of $\leq 10^{-6} \text{ cm}^{-3}$ far away of clusters. Adiabatic compression and internal shocks of the converging flow within these sheets onto clusters of galaxies should heat the gas further to the above temperatures of 0.5 – 1 keV.

During the passage through the shock, the magnetic fields are amplified and aligned with the shock plane. The radio emission of a relic should therefore exhibit polarization properties depending on the viewing angle. Assuming a spherical accretion shock with a radius depending on the depth of the cluster potential, the viewing angle and the resulting polarization can be estimated (Fig. 3). These agree well with measured polarizations for relics in two clusters: 1253+275 in Coma, and 1712+64 in A2255. For 0917+75 in A786, the large projected radius would imply a deep gravitational potential and therefore a very high

cluster temperature, which is not yet measured. 0917+75 might also trace an accretion shock of the stream onto the supercluster Rood #27, which A786 is a member of. This could also explain the large apparent radius of the relic.

In case of 1706+78 in A2256 the measured polarization exceeds the expected one significantly, indicating that the viewing angle is much higher than if the relic were located at the accretion shock. A consistent shock radius would be $1 \text{ Mpc } h_{50}^{-1}$, which means that an internal shock of the cluster powers the relic, which should result from a highly developed merger event. Roettiger et al. (1995) discuss several apparent signs of such an event in A2256, and fit simulations to the X-ray data. Their best-fit value of the angle between the merger axis and the line-of-sight within our theory of field compression predicts exactly the observed polarization.

The directions of the projected magnetic fields are roughly perpendicular in all above examples to the direction pointing to the cluster center, as is expected.

For the other five relics of our sample no polarization measurements are available. We predict $\approx 30\%$ polarization for 2006-56 in A3667, $\approx 10\%$ for 2010-57 in A3667, and less than 5% for 0038-096 in A85, 1140+203 in A1367, and 1401-33 in S753. Polarization measurements of these sources could verify the existence of cluster accretion shocks and help us to reveal an important piece of the cosmological structure formation puzzle.

The time elapsed since the magnetized plasma has started to pass the shock can be calculated in two independent ways. Both estimates give ages of the order of some 10^8 yr, and are therefore a further justification of our model.

Since our sample contains mostly relics seen under viewing angles below 60° , we expect that more relics might be discovered in the outer regions of clusters. Any radio search within these large areas should be guided by the expected correlation of the large-scale structure filaments and typical inflow directions into clusters.

We conclude that the properties of cluster radio relics are naturally explained if they are understood to trace some of the giant shock fronts of the cosmological large-scale motion of the on-going structure formation. This demonstrates for the first time the existence of these theoretically predicted shocks. Estimated magnetic fields, temperatures and densities of the accreting matter fit into the structure formation scenario.

Acknowledgments. We would like to thank H. Kang, D. Ryu for extensive discussions on large-scale structure formation, Gopal Krishna for discussions on radio relics, and the referee, L. Feretti, for useful comments and advice which helped to improve the presentation of our work. We further acknowledge G. Giovannini, L. Feretti and C. Stanghellini for the permission to use their figure. TAE acknowledges financial support by the *Studienstiftung d.*

dt. Volkes. This research has made use of the NASA/IPAC Extragalactic Database (NED) which is operated by the Jet Propulsion Laboratory, California Institute of Technology, under contract with the National Aeronautics and Space Administration.

References

- Andernach H., Feretti L., Giovannini G., 1984, A&A 133, 252
 Biermann P.L., 1993, A&A 271, 649
 Biermann, P.L., 1996, In: Jokipii J.R., et al. (eds.) Cosmic Winds and the Heliosphere. University of Arizona Press, Tucson, in press
 Biermann P.L., Kang H., Rachen J.P., Ryu D., 1997, In: Proc. Moriond Meeting on High Energy Phenomena, Les Arcs, in press
 Bird C.M., Mushotzky R.F., Metzler C.A., 1995, ApJ 453, 40
 Blumenthal G.R., Gould R.J., 1970, Rev. Mod. Phys. 42, 237
 Bridle A.H., Fomalont E.B., 1976, A&A 52, 107
 Briel U.G., Henry J.P., Schwarz R.A., et al., 1991, A&A 246, L10
 Briel U.G., Henry J.P., Böhringer H., 1992, A&A 259, L31
 Burn B.J., 1966, MNRAS 133, 67
 Burns J.O., Roettiger K., Pinkney J., Perley R.A., Owen F.N., 1995, ApJ 446, 583
 Colberg J.M., White S.D.M., Jenkins A., Pearce F.R., preprint, astro-ph/9711040
 David L.P., Slyz A., Jones C., et al., 1993, ApJ 412, 479
 David L.P., Jones J., Forman W., 1995, ApJ 445, 578
 Deiss B.M., Reich W., Lesch, H., Wielebinski R., 1997, A&A 321, 55
 Drury L.O'C., 1983, Rep. Prog. Phys. 46, 973
 Drury L.O'C., Markiewicz W.J., Völk H.J., 1989, A&A 225, 179
 Enßlin T.A., Biermann P.L., Kronberg P.P., Wu X.-P., 1997, ApJ 477, 560
 Enßlin T.A., Biermann P.L., 1998, A&A, in press, scheduled for A&A 330, 90, astro-ph/9709232
 Fabian A.C., Daines S.J., 1991, MNRAS 252, 17
 Fadda D., Girardi M., Giuricin G., Mardirossian F., Mezzetti M., 1996, ApJ 473, 670
 Feretti L., Perola G.C., Fanti R., 1992, A&A 265
 Feretti L., Dallacasa D., Giovannini G., Tagliana A., 1995, A&A 302, 680
 Feretti L., Giovannini G., 1996, In: R. Ekers, C. Fanti & L. Padrielli (eds.) IAU Symp. 175, Extragalactic Radio Sources. Kluwer Academic Publisher, p. 333
 Feretti L., Böhringer H., Giovannini G., Neumann D., 1997, A&A 317, 432
 Fontanelli P., 1984, A&A 138, 85
 Gavazzi G., 1978, A&A 69, 355
 Gavazzi G., Trinchieri G., 1983, ApJ 270, 410
 Gavazzi G., Jaffe W., 1987, A&A 186, L1
 Gavazzi G., Contursi A., Carrasco L. et al., 1995, A&A 304, 325
 Giovannini G., Feretti L., Andernach H., 1985, A&A 150, 302
 Giovannini G., Feretti L., Stanghellini C., 1991, A&A 252, 528
 Goldschmidt O., Rephaeli Y., 1994, ApJ 431, 586
 Goss W.M., Ekers R.D., Skellern D.J., Smith R.M., 1982, MNRAS 198, 259

- Goss W.M., McAdam W.B., Wellington K.J., Ekers R.D., 1987, *MNRAS* 226, 979
- Hanisch R.J., 1980, *ApJ* 85, 1565
- Harris D.E., Stern C.P., Willis A.G., Dewdney P.E., 1993, *AJ* 105, 769
- Harris D.E., Willis A.G., Dewdney P.E., Batty J., 1995, *MNRAS* 273, 785
- Honda H., Hirayama M., Watanabe M., et al., 1996, *ApJ* 473, L71
- Jaffe W.J., 1992, In: Fabian A.C. (ed.), *Clusters and Superclusters of Galaxies*. Kluwer Academic Publisher, Dordrecht, p. 109
- Jones C., Forman W., 1984, 276, 38
- Joshi M.N., Kapashi V.K., Bagchi J., 1986, In: O’Dea C.P. & Uson J.M. (eds.) *NRAO Proc., Radio Continuum Processes in Clusters of Galaxies*. Green Bank, p. 73
- Kang H., Ryu D., Jones T.W., 1996, *ApJ* 456, 422
- Kang H., Rachen J.P., Biermann P.L., 1997, *MNRAS* 286, 257
- Kim K.-T., Kronberg P.P., Dewdney P.E., Landecker T.L., 1986, In: O’Dea C.P. & Uson J.M. (eds.) *NRAO Proc., Radio Continuum Processes in Clusters of Galaxies*. Green Bank, p. 199
- Kim K.T., Kronberg P.P., Giovannini G., Venturi T., 1989, *Nature* 341, 720
- Kim K.T., Tribble P.C., Kronberg P.P., 1991, *ApJ* 379, 80
- Knopp G.P., Henry J.P., Briel U.G., 1996, *ApJ* 472, 125
- Landau L.D., Lifschitz E.M., 1966, *Hydrodynamik*. Akademie-Verlag, Berlin
- Lima Neto G.B., Pislar V., Durret F., Gerbal D., Slezak E., 1997, *A&A* 322, 53
- Markevitch M., 1996, *ApJ* 465, L1
- Markevitch M., Sarazin C.L., Henriksen, M. J. 1996 In: *X-ray Imaging and Spectroscopy of Cosmic Hot Plasmas*, Tokyo, astro-ph/9606113
- Markevitch M., Forman W., Sarazin C.L., Vikhlinin A., 1997, *ApJ*, submitted, astro-ph/9711289
- Navarro J., Frenk C.S., White D.M., 1995, *MNRAS* 275, 720
- Parma P., de Ruiter H.R., Mack K.-H., et al., 1996, *A&A* 311, 49
- Rephaeli Y., Ulmer M., Gruber D., 1994, *ApJ* 429, 554
- Reynolds J.E., 1986, In: O’Dea C.P. & Uson J.M. (eds.) *NRAO Proc., Radio Continuum Processes in Clusters of Galaxies*. Green Bank, p. 59
- Roettiger K., Burns J.O., Pinkney J., 1995, *ApJ* 453, 634
- Röttgering H., Snellen I., Miley G., et al., 1994, *ApJ* 436, 654
- Röttgering H., Wieringa M.H., Hunstead R.W., Ekers R.D., 1997, *MNRAS* 290, 577
- Ryu D., Kang H., 1997, *MNRAS* 284, 416
- Schlickeiser R., Sievers A., Thiemann H., 1987, *A&A* 182, 21
- Slee O.B., Siegman B.C., 1983, *Proc.ASA* 5, 114
- Slee O.B., Roy A.L., Savage A., 1994 *AuJPh* 47, 145
- Sodré L., Capelato H.V., Steiner J.E., Proust D., Mazure A., 1992, *MNRAS* 259, 233
- Venturi T., Feretti L., Giovannini G., 1988, *A&A* 213, 49
- Völk H.J., 1997, to appear in *Kruger Park Workshop Proceedings: 1997*, astro-ph/9711204
- Wang Y., Biermann P.L., 1997, *A&A*, submitted
- Webb G.M., Drury L.O’C., Biermann P.L., 1984, *A&A* 137, 185
- White S.D.M., Briel U.G., Henry J.P., 1993, *MNRAS* 261, L8
- Wiebel-Sooth B., Meyer H., Biermann P.L., 1997, *A&A* (in press), astro-ph/9709253
- Zabludoff A.I., Geller M.J., Huchra J.P., Vogeley M.S., 1993, *AJ* 106, 1273